Design of a high-quality multi-terminal semiconductor switch

Juan Daniel Torres Luna

TU Delft

Design of a high-quality multi-terminal semiconductor switch

by

Juan Daniel Torres Luna

to obtain the degree of Master of Science
at the Delft University of Technology,
to be defended publicly on March 11st

Student number:	5213983	
Project duration:	August 31, 2021 – March 2, 2022	
Thesis committee:	Prof. Michael Wimmer,	TU Delft, supervisor
	Prof. Anton Akhmerov	TU Delft, co-supervisor
	Prof. Srijit Goswami	TU Delft

TU Delft

Contents

1 Background

1.1. Introduction

Majorana bound states (MBS) can be used to store quantum information protected from the local environment. Majorana based quantum computation requires controlled interaction of multiple MBS in a two dimensional device. There are many proposals for Majorana qubit, but most of them rely on phenomenological models that ignore microscopic details.

MBS can be realised by combining multiple materials with different interactions in a quasi-one dimensional system, i.e. a nanowire. The ingredients for creating Majoranas are: strong spin-orbit semiconductor, proximity induced superconductivity, and a magnetic field along the nanowire axis.

Devices with multiple Majoranas require multiple parallel nanowires coupled using semiconducting structures. For example, nanowire or gate-defined networks in 2DEGs have been studied experimentally and theoretically as platforms for Majorana based computation. In such a device, the ground state evolves by selectively coupling different MBS pairs. While coupling a single MBS pair can be done using a quantum dot, selective coupling of multiple pairs remains a challenge. On one hand, there are geometrical constraints given by tuning multiple separate nanowires in the topological phase. On the other hand, the coupling of multiple pairs should be optimised simultaneously by the device geometry. Therefore, design of a multi Majorana device requires consideration of the microscopic and geometric details.

The simplest system where multiple MBS can couple non-trivially is in a trijunction geometry. In a ballistic system, the geometrical details of the trijunction determine entirely the coupling of multiple pairs. Furthermore, in a realistic device, such as a 2DEG, the trijunction geometry is implemented by electrostatic gates as a potential landscape. In this context, this work explores the geometrical dependence of selectively coupling multiple MBS pairs in a Majorana trijunction.

1.2. Majorana bound states

MBS populate the non-local degenerate ground state of a topological superconductor [8]. Under the appropriate conditions, a spinless one-dimensional p-wave superconductor contains two zero-energy excitations that are exponentially localised at the edges of the system.

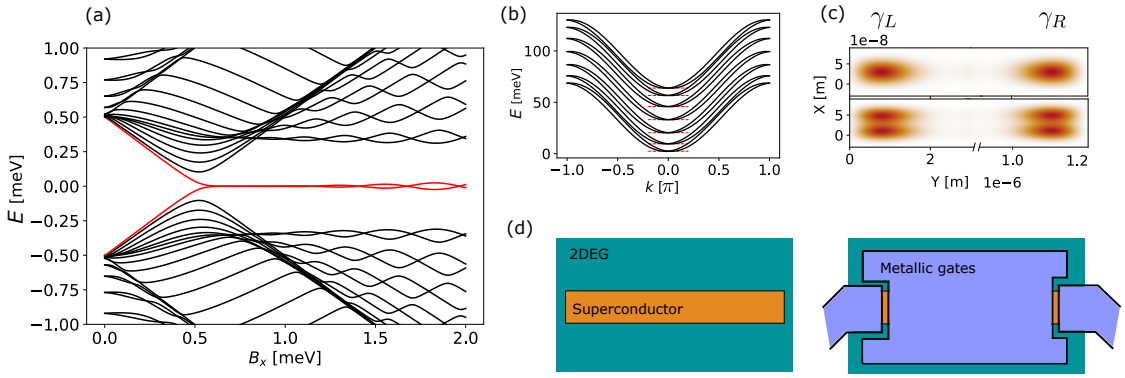

Figure 1.1: Simulations of a Majorana nanowire as described in Eq. (1.4). The following parameters will be used in all simulations: $\Delta = 0.5$[meV], $\alpha = 0.3$[eV A], and $m^* = 0.023 m_e$. Each simulated nanowire has length $L = 1.3$ [μm] and width $W = 70$ [nm]. (a) Topological phase transition as a function of Zeeman field B_x. Lowest mode (red) sticks to zero after crossing the critical field. (b) Transverse bands along the translational invariant direction with $\Delta = 0$. The chemical potential is tuned to the bottom of each band (red dashed lines) to create Majoranas. (c) Majorana wavefunctions for the lowest two bands. (d) Illustration of how a Majorana nanowire is built on a 2DEG. Left panel shows the 2DEG with a superconducting stripe on top. Right panel shows the system after the deposition of the gates.

These two zero modes encode a single fermionic mode that can be empty or occupied,

$$f = \frac{\gamma_L + i\gamma_R}{\sqrt{2}}, \quad f^\dagger = \frac{\gamma_L - i\gamma_R}{\sqrt{2}}, \tag{1.1}$$

where $\gamma_i = \gamma_i^\dagger$ are Majorana operators that satisfy $\{\gamma_i, \gamma_j\} = 2\delta_{ij}$.

In a sufficiently long nanowire, MBS are decoupled from each other, and noise sources will interact with each of them individually. The interaction with a single MBS is proportional to a single Majorana operator, i.e. $\gamma \sim f + f^\dagger$, and thus it will change the parity of the system. In a superconductor, however, electrons can only enter or leave as Cooper pairs, which means that the parity is conserved. Therefore, individual MBS are immune to local noise sources.

Consequently, only even powers of Majorana operators are allowed in the Hamiltonian. The simplest allowed term describes the coupling of a pair of MBS. In a single nanowire, or in a linear array of them, it is only possible implement this term with successive MBS. It is given by,

$$H_{pair} = iE_{LR}\gamma_L\gamma_R = E_{LR}(1 - 2f^\dagger f). \tag{1.2}$$

Here, E_{LR} is the tunnelling coupling between the two MBS. Consequently, a general state within the degenerate subspace evolves as,

$$|\Psi\rangle = \alpha|0\rangle + \beta|1\rangle \rightarrow U(t)|\Psi\rangle = \alpha|0\rangle + \beta e^{2iE_{LR}t}|1\rangle. \tag{1.3}$$

However, universal quantum computation cannot be built from using only quadratic fermionic terms [21] as in Eq. 1.2. Controlled interaction between at least three MBS from different fermions is essential to Majorana based quantum computation [4, 11, 18]. Therefore, a higher dimensional structure where multiple MBS converge is required in order to do Majorana computation.

1.3. Experimental platforms

The Hamiltonian that realises a Majorana nanowire [1] is,

$$\mathcal{H} = \sum_k \Psi_k^\dagger H(k) \Psi_k, \quad H(k) = \left[\frac{|\mathbf{k}|^2}{2m^*} - \mu + \alpha(k_x \sigma_y - k_y \sigma_x) \right] \tau_z + B_x \sigma_x + \Delta \tau_x. \tag{1.4}$$

Here, $\Psi_k^\dagger = (f_{k\uparrow}^\dagger, f_{k\downarrow}^\dagger, f_{k\uparrow} f_{k\downarrow})^T$ are the Nambu spinors in k space, μ is the chemical potential, $\mathbf{k}$ is the 2D wave-vector, α is the spin orbit interaction, B_x is the Zeeman field, Δ is the superconducting gap, and σ and τ are Pauli matrices for the spin and particle-hole basis. MBS appear as zero energy excitations of this Hamiltonian when $B_x^2 \geq \sqrt{\mu^2 + \Delta^2}$.

Creating and unambiguously detecting MBS is a challenge. On the one hand, the required interactions compete with each other [17], e.g. superconductivity and magnetic field, requiring fine tuning. On the other hand, MBS signatures can be reproduced by states localised in material defects or impurities [12, 22]. Consequently, most of the current work in this field is focused on unambiguously finding a single MBS pair.

Truly one-dimensional systems do not exist. There is a translational invariant direction, and at least one direction with finite width W. The energy of each mode has a contribution from both, and it is given by,

$$E_n(k) = \frac{\hbar^2}{2m^*} \left(k^2 + \frac{\pi^2 n^2}{W^2} \right). \tag{1.5}$$

Here, m^* is the effective mass and the spin orbit splitting is not considered. Independent MBS with different momentum profiles can be formed at each transverse mode [13] when the chemical potential is at the bottom of the corresponding band.

1.3.1. Two dimensional electron gases

In order to build a multi Majorana device we require a 2D platform where multiple nanowires can be easily attached. 2DEGs are an interesting candidate for multi Majorana devices since arbitrary geometries can be created using electrostatic gates. On the other hand, high-quality networks of semiconducting nanowires can be built [7], but geometries are limited to straight configurations.

Parallel Majorana nanowires are the basic elements for a complex Majorana device. A single nanowire on a 2DEG can be created by adding a superconducting strip on top of the selected region as shown in Fig. 1.1 (d). Then, a top gate is deposited next on top of the device such that depletes the surrounding 2DEG. A narrow quasi-one dimensional channel is created below the superconductor where the gate electric field is screened [6]. Following this procedure, multiple parallel nanowires can be created in a 2DEG by selectively depositing superconducting covers.

There are several Majorana experiments on 2DEGs that have shown promising evidence for scalable and complex devices. Initial experiments [9, 19] focused on characterising the properties of semiconducting layers with a superconducting cover. Advances in material growth allowed for clean interfaces with a hard superconducting gap to develop into the nanowire region. Later experiments focused on tunnel spectroscopy of stripe-like geometries [20] where a zero bias peak (ZBP) was found. However, due to disorder and defects such ZBPs have most likely a trivial origin from Andreev states rather than MBS. Nevertheless, efforts to develop complex devices in 2DEGs are made and new promising materials are being studied [14].

1.3.2. Electrostatic gates

The potential landscape in a 2DEG can be controlled by deposition of metallic gates on a top layer with an insulating barrier in between that smooths the potential profile [2]. The electrostatic potential in a 2DEG is found by solving the Poisson equation using a finite elements method [3] on the device geometry. The potential landscape, $U(\mathbf{r})$, for a given geometrical configuration can be found by solving Laplace equation,

$$\nabla \cdot [\varepsilon_r(\mathbf{r}) \nabla U(\mathbf{r})] = 0. \tag{1.6}$$

Here, ε_r is the relative permittivity of each layer in the material stack. In general, the quantum electrostatics problem is more complicated due to the interaction of dopant charges with the potential. However, our problem is simpler since no extra charges are required.

1.4. Majorana bound states in a trijunction

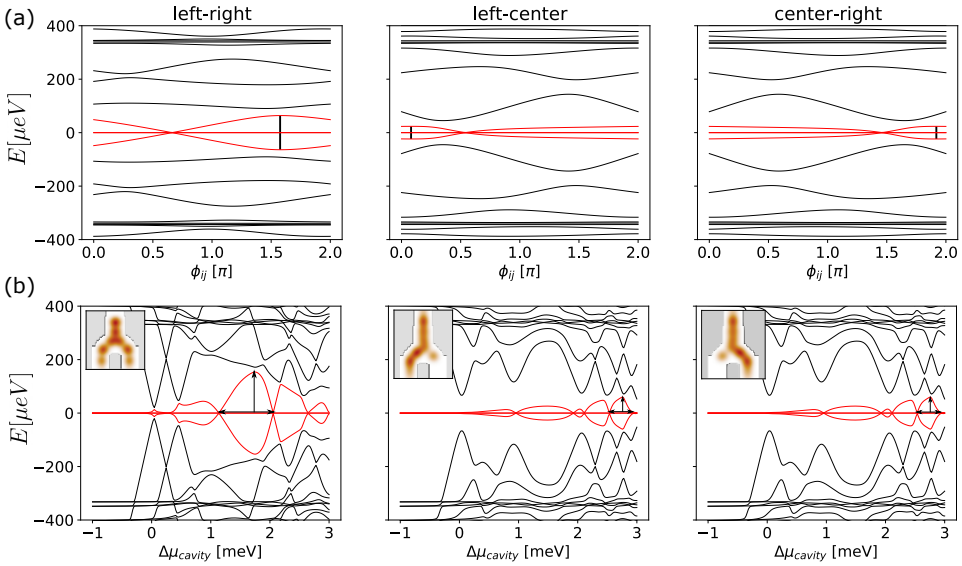

Figure 1.2: Example of a Y-shaped trijunction. Spectra as a function of (a) superconducting phase difference and (b) cavity chemical potential difference for the coupling of each pair. Lowest two modes are highlighted in red. The mode that remains at zero describes the MBS at the far ends of the nanowires. The mode that acquires a finite coupling corresponds to the coupled MBS. Vertical black lines in (a) indicate where the coupling reaches a maximum. Vertical and horizontal arrows in (b) indicate the height and width of the largest resonant peaks. Insets in (b) show representative coupled MBS wavefunctions. Typical distance between nanowires is 200 nm.

In order to create a Majorana qubit, at least three MBS with local pair interactions are required [1]. The device that realises this selective coupling is called a trijunction. It is defined using gates placed on top of a 2DEG, and it is operated by controlling the voltages of the different gates. It contains two parts: three nanowires, and a central cavity that mediates the coupling. Both systems are described by Eq. (1.4), but the cavity has no superconducting cover, i.e. $\Delta = 0$ in the cavity. In such a system, demonstration of the simplest non-trivial Majorana evolution experiment can be done. The geometrical configuration of the trijunction is subject to two main constraints: On one hand, nanowires must be parallel since the topological phase closes for small deviations of the magnetic field. On the other hand, nanowires must have a significant separation from each other such that MBS are

well isolated. Consequently, the design of a trijunction geometry with selective coupling between MBS pairs requires a systematic study of the geometry dependence.

The basic operation of a trijunction is shown in Fig. 1.2. We simulate the pair coupling of three Majorana nanowires mediated by a semiconducting cavity using Kwant [5]. For each experiment, a pair of nanowires is set to host MBS in each sub band while the other nanowire is depleted. The coupling energy of each pair is extracted as the value of the lowest non-zero eigenvalue with respect to the phase difference Fig 1.2 (a) or cavity chemical potential Fig 1.2 (b). The phase difference between the selected nanowires is tuned such that the coupling is at a maximum (see black vertical lines in Fig. 1.2 (a)). Observe that the phase shift is symmetric with respect to π. Given the symmetry of the system, the coupling of the central pairs is the same, and thus we calculate only one of them.

Previous trijunction designs [6] have studied MBS coupling in the tunnelling regime. In this context, the MBS coupling relies entirely on wavefunction overlap along the cavity. Consequently, MBS pairs acquire relatively small couplings with the advantage of not introducing any extra sub gap state.

On the other hand, in the strong coupling regime (Fig 1.2 (b)) the MBS coupling is mediated by cavity states but with extra levels present inside the gap. Nevertheless, the coupling energy of the MBS pairs can become significantly larger, i.e. comparable with the induced gap. The modulation of the coupling now relies on the cavity geometry. Interestingly, it has been shown that properties Majorana devices can be optimised by using geometrical effects [10]. Particularly, a zig-zag geometry enhances the MBS localisation by cutting long trajectories that populate a straight geometry.

2

Trijunction of Majorana nanowires

In this chapter we demonstrate that the coupling of three pairs of MBS in a trijuction is determined by the geometrical details of the central semiconducting cavity. For certain geometrical configurations, a MBS pair couples resonantly with successive cavity states as in the so-called *resonant trapping*, while in other cases the coupling is mediated by individual non-overlapping levels.

The basic operation of the trijunction follows the procedure described in Fig. 1.2. We consider the strong coupling regime where there are no tunnel barriers between the cavity and the nanowires. The cavity chemical potential is varied in a range of 4 meV around the first resonance for all cavities. In this range, there are multiple levels that couple resonantly with a given pair of MBS. In order to characterise the coupling, we extract the highest resonance peak for each geometry as indicated by the black arrows in Fig. 1.2 (b). Then, we classify them according to their operational robustness, that is, height and width.

2.1. Quasi-one dimensional cavities

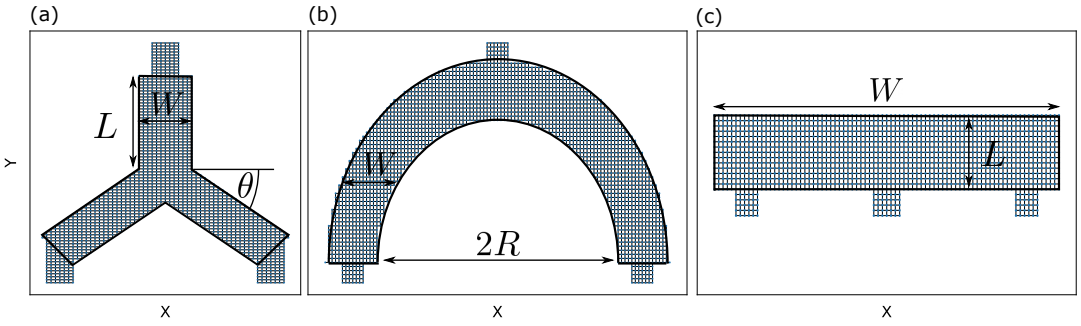

Figure 2.1: Kwant systems describing the three quasi-1D cavities: (a) Y-shaped defined by three parameters: arms length and width, L and W, and lateral arms angle θ. (b) Half-ring defined by the radius R and the width W. (c) Rectangular stripe defined by the length L and width W.

Consider a quasi-1D cavity with mirror symmetry around the y-axis. The position of the three nanowires is fixed: one is attached at the center, and one at each end. Consequently, the phase shift for the central MBS pairs is symmetric around π as in Fig. 1.2 (a). Similarly, the coupling of the left-center MBS pair and center-right MBS pair is the same as in Fig.

1.2 (b). Under these constrains, we study how the geometry affects the coupling of the two different pairs.

We consider three cavity geometries: In Fig. 2.1 (a) one can observe a Y-shaped cavity. In Fig. 2.1 (b) one can observe a half-ring stripe cavity with three nanowires attached in a fork-like geometry. In Fig. 2.1 (c) one can observe a rectangular stripe cavity with three Majorana nanowires attached.

2.1.1. Trijunction performance with respect to system size

Initially, the overall size of the system is varied, and a transition from the small to the long junction regime is found for all geometries. In Fig. 2.2 one can observe the evolution of the largest resonance peak for each geometry as a function of the system size.

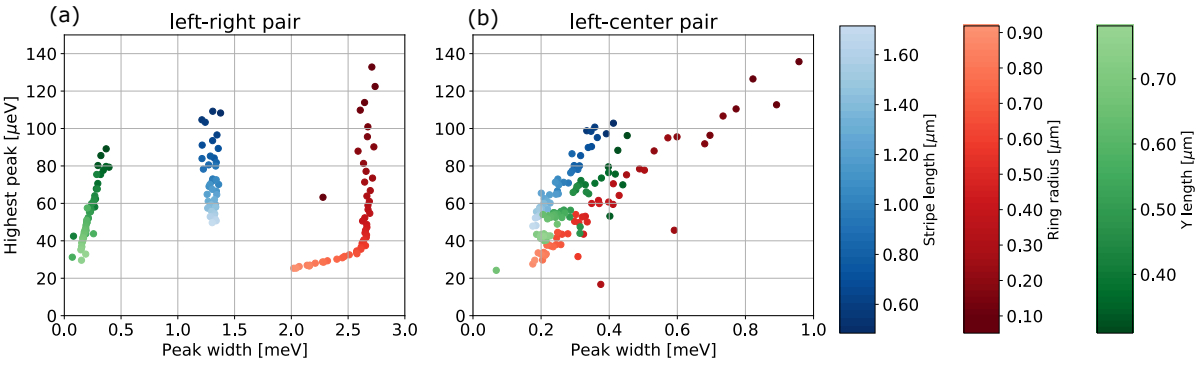

Figure 2.2: Geometrical dependence of the resonant coupling peaks for three quasi-1D geometries that correspond to each colorbar. The system is tuned to the lowest Majorana band. (a) Left-right MBS pair coupling. (b) Left-center MBS pair coupling.

The coupling of the left and right MBS pair shows a clear geometrical dependence as can be observed in Fig. 2.2 (a). Each geometry occupies a separate region in the resonant height-width plane. The ring cavity has the most robust resonant peaks. For small R, the coupling is larger than any other geometry. Similarly, the width is the largest, and it persists even for rings with diameter 1 μm after which decays. Then follows the stripe geometry that has approximately the same width for all considered geometries. Finally, the Y-shaped cavity has overall the smallest resonant peak width.

The coupling of the central MBS pairs, on the contrary, cannot be easily separated for each geometry. Generally, one can see three diagonal stripes in Fig. 2.2 (b) where the stripe geometry has the largest resonant peak height. The peak width decreases as the size increase, and it has the same slope for all geometries. Nevertheless, for sufficiently small sizes, the ring geometry has peak heights and widths larger than any other geometry.

We have found that there is systematic difference in the resonance peak width for different quasi-1D geometries. A large coupling can be found for reasonably large devices, e.g. nanowire separation around 1 μm.

2.1.2. Resonant trapping

Consider the half-ring cavity. When the left and right nanowires are close to the ends of the cavity, the MBS pair couple along a sequence of overlapping resonant states as can be seen in the blue line of Fig. 2.3 (a). The cavity states interfere constructively and the coupling accumulates creating a single wide peak over the resonant region. It depends crucially on

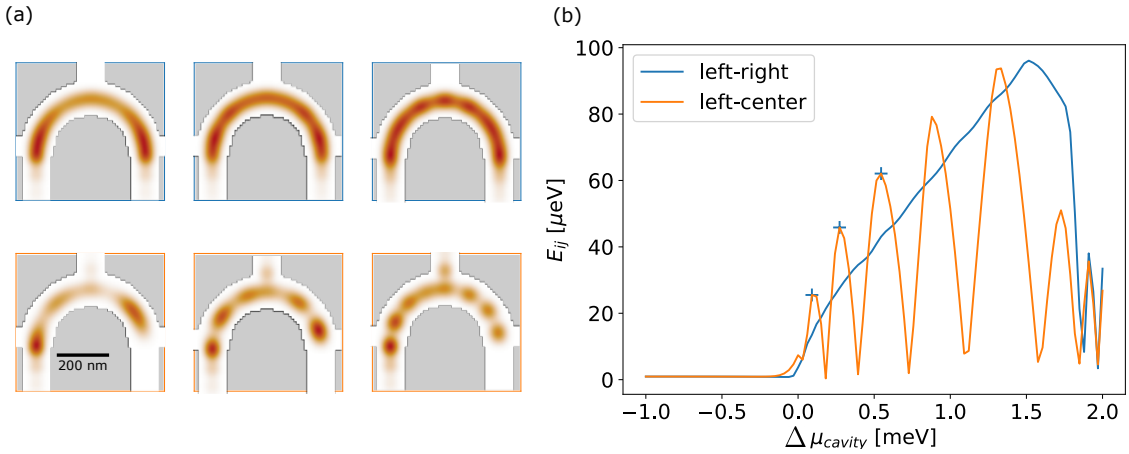

Figure 2.3: Spectra for a half-ring shaped cavity of width $W = 110$ [nm] and radius $R = 300$ [nm]. The system is tuned to the lowest Majorana band. (b) Coupling of each MBS pair. Center-right pair is the same curve as left-center pair. Crosses indicate the positions at where the wavefunction (a) are taken. The color of the frame in (a) corresponds each MBS pair in (b).

having the lead states around all of the cavity wavefunction as can be seen in Fig. 2.3 (b). This phenomena is known as *resonant trapping* [15, 16].

For the central pairs coupling, in contrast, a band of resonances cannot form since the cavity wavefunction is not fully enclosed. When coupling the left and central MBS, the cavity region close to the right lead acts as a particle in a box with multiple individual levels that repel each other. Consequently, we observe the orange line shown in Fig. 2.3 (a) where the resonant band is divided in individual resonances.

The difference when coupling multiple MBS pairs relies on the geometric configuration of the cavity wavefunctions and the MBS relative positions. Then, one can explain the distribution of couplings observed in Fig. 2.2. The left and right MBS in the ring and stripe geometry have an approximately constant and large widths over the different system sizes because cavity levels remain resonant. On the other hand, the coupling of the central MBS pairs in any geometry has a much smaller width because some part of the wavefunction is not coupled. Particularly, the Y-shaped junction has a small width for all pairs because no resonant trajectories can be created in such geometry.

2.2. Two dimensional cavities

In a ballistic cavity, the motion of the electrons is determined by the shape of the cavity and leads. The electrons follow semiclassical trajectories connecting different leads that can be identified as peaks in the conductance [23]. Following such intuition, we explore if changes in the geometry of a 2D cavity can be used to modulate the coupling of different MBS pairs. Particularly, we explore how the angular dependence of the incoming modes, and internal angles of the cavity, influence the MBS coupling.

We consider three geometries: In Fig. 2.4 (a) one can observe a circular cavity with Majorana nanowires attached in a fork-like geometry. In this geometry one can control the angle of the incoming MBS. In Fig. 2.4 (b) one can observe a triangular cavity with nanowires attached at the lower side. In this geometry one can control the angle of MBS scattering within the cavity by changing the diagonal sides. In order to explore to role of the positioning of the leads, we explore a variation of the triangular geometry with the central

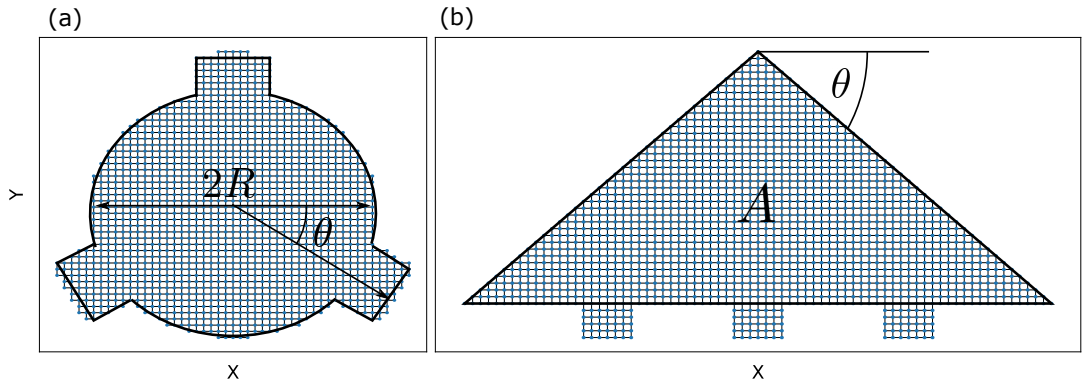

Figure 2.4: (a) Kwant system of a circular shaped cavity. It is defined by the radius R and the angle of the leads θ. (b) Kwant system of a triangular shaped cavity. It is defined by the total area A and the angle of the diagonal sides θ.

lead in the top side. Lastly, we consider a rectangular geometry that can be created by extending the length of the stripe geometry shown in Fig. 2.1 (c).

2.2.1. Trijunction performance with respect to system size

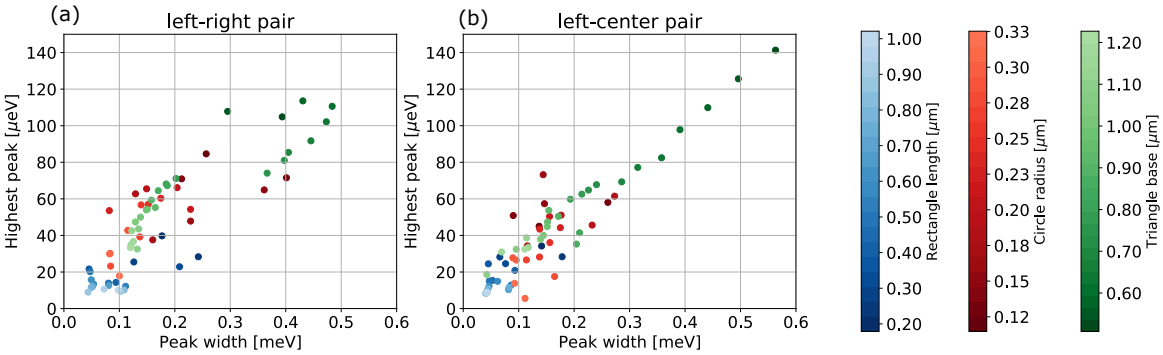

Figure 2.5: Size dependence of the three 2D geometries considered in this section corresponding to each colorbar. The system is tuned to the lowest Majorana band. The (a) left right and (b) left center largest resonant peaks are shown. The angle of all the cavities here is $\theta = \pi/4$.

In Fig. 2.5 one can observe the size dependence of the resonant peak for the three two-dimensional geometries considered. Overall, there is no major distinction between the coupling of different pairs. All couplings decays as the system size increases following a diagonal line in Fig. 2.5 panels (a) and (b). Nevertheless, the geometry dependence can be seen in three different regions along the diagonal.

On the rightmost region, one observes that the triangular geometry has the largest couplings and widths for small sizes. Descending along the diagonal, the triangular and circular geometries overlap. Remarkably, there is a significant size difference between them in the overlapping region, approximately 500 nm. Most of circular geometries are concentrated in this region. At the bottom of the diagonal, one observes that the worst MBS couplings happen for rectangular geometries.

Unlike quasi-1D geometries, the size dependence 2D geometries considered does not have a clear boundary. Nevertheless, a large coupling can be found for reasonably large devices in the case of the triangular cavity.

2.2.2. Trijunction performance with respect to cavity angle

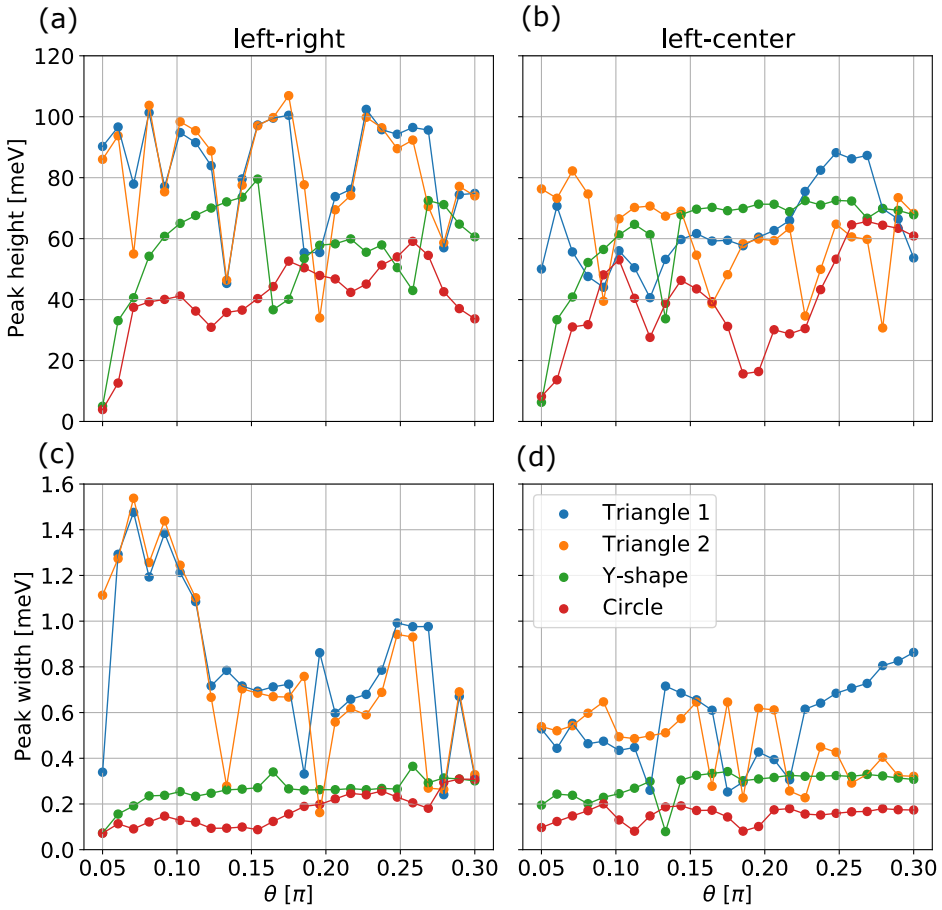

Figure 2.6: Angular dependence of the resonant coupling peaks for four geometries with angle dependence. The system is tuned to the lowest Majorana band. Peak height and width for (a, c) left-right MBS pair and (b, d) left-center MBS pair coupling. The dimensions (base × height) of the triangle vary between 1×0.15 μm for small angles up to 0.4×0.5 μm for large angles. The radius of the circular cavity is $R = 250$ [nm]. The size of the Y-shaped cavity is similar to that of the triangular cavity.

The angle is varied in two triangular cavities, one circular cavity, and the Y-shaped cavity. The resulting coupling for each pair and geometry is shown in Fig. 2.6. In Fig. 2.6 (a) one can observe that there is a large variation of the peak height, yet there are angle ranges where the coupling stays approximately constant. In Fig. 2.6 (c) one can observe two different regions in the resonant peak width. For small angles, the width is large, but as the angle increases the width drops. In these two figures we observe a transition from the resonant trapping regime to the single resonance regime while maintaining an approximately constant peak height. Note that for small angles the triangular cavity resembles a quasi-1D system. By cutting the edges of the stripe geometry, the wavefunction concentrates around the center such that it is easily trapped between the left and right leads as observed in the blue curve of Fig. 2.7 (a). As the angle increases, the resonant band splits into several sub bands that contain a few resonances each as observed in Fig. 2.7 (b).

The coupling of the left and central MBS pair for the triangular geometries shown in Fig. 2.6 (b) and (d) shows no systematic behaviour. Nevertheless, one observes in Fig. 2.6 (b) that the configuration with wires at the lower side (blue dots) has a maximum at large angles, while the configuration with wires at both sides has a maximum at small angles.

Furthermore, by comparing peak height around these two peak in Fig. 2.6 (a) and (b), one observes that both are in the range 80−100 μeV. Therefore, there are two triangular configurations where the coupling of all pairs reaches a similar value. Note, however, that the small angle configuration would be rather considered a quasi-1D system since the ratio between its dimensions.

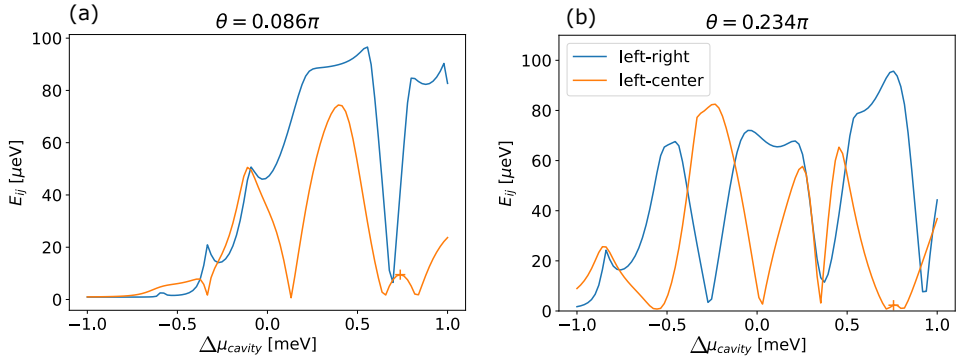

Figure 2.7: Coupling of triangular geometries with the central lead at the (a) top and (b) bottom sides.

For the remaining geometries, there is indeed a modulation for the left and right MBS pairs. The overall coupling is comparable to the triangular geometries, but the width is much smaller. The left and central MBS coupling for the Y-shaped cavity converges to a peak height of about 70 meV as the angle increases (see Fig. 2.6 (c) green points). The circular geometry shows that different angles enhance the coupling of different pairs as can be seen in the red lines.

The angular dependence does not show a systematic difference for the triangular geometries, but it does for the Y-shaped cavity. However, for devices with similar size, the resonant peak height has a large difference between geometries, and the triangular geometry dominates.

2.2.3. Majorana sub bands

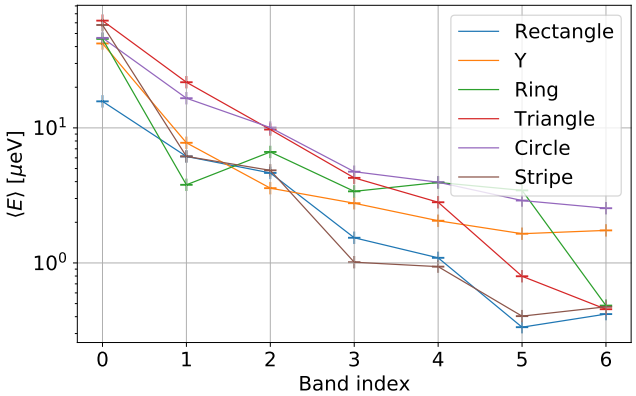

Figure 2.8: Mean geometry-pair coupling for all Majorana sub band and all geometries considered in this section. The geometry average is taken over the data shown in Fig. 2.5.

By tuning each nanowire sub band into the topological phase, we probe the momentum distribution of the cavity states. In Fig. 2.8 one can observe the mean coupling for each

band. It has been averaged over all geometrical configurations and all MBS pairs since no clear distinction between them is found.

Overall, the coupling decays exponentially as the band index increases. The decay is modulated by the geometry, but the trend holds in all cases. There is, approximately, two order of magnitude decrease in the coupling from the lowest to the highest band.

The lowest band carries the largest coupling. This allows us to infer that the momentum distribution of cavity states is dominated by low momentum states. This behaviour is expected to change in the presence of disorder due to coupling of different momentum channels. However, a precise quantitative description of the momentum profiles and the presence of disorder goes beyond the scope of this work.

3

Gate-defined triangular cavities

In this chapter, we simulate a gate defined triangular cavity and describe its operation as a switch that couples different MBS pairs. The device is built using a stack with three layers of materials: 2DEG, dielectric and metallic gates. The electrostatic potential inside the 2DEG is found as the solution to Eq. (1.6) using the finite element solver from Ref. [3].

Two devices are simulated in order to study the angular dependence previously found. First, we discuss the tuning of each device such the potential resembles the triangular cavity and the nanowires are strongly coupled. Then, the MBS coupling is calculated and compared to the purely geometric case.

3.1. Gates configuration

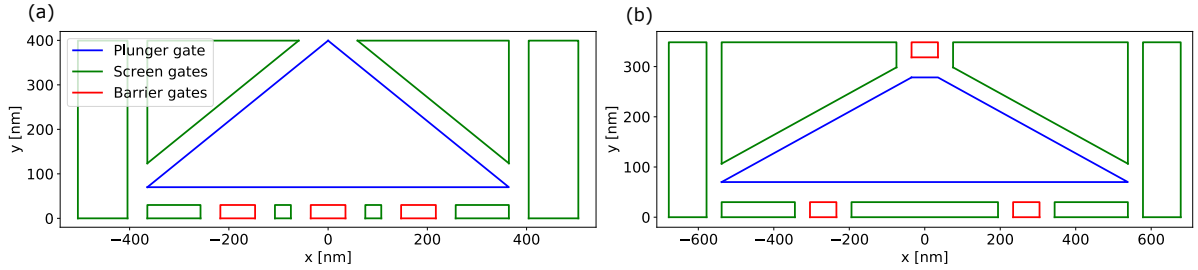

Figure 3.1: Gate configuration of the two triangular cavities considered. (a) Triangular cavity with angle $\theta = 0.234\pi$ with all nanowires at the lower side. (b) Triangular cavity with angle $\theta = 0.125\pi$ with central nanowire at the top side. Spacing between gates is set to 40 nm. Barrier gates have length 30 nm and width 70 nm. Nanowires (not shown) are attached at the ends of the barrier gates. The vertical configuration includes a 2DEG of thickness 40 nm. Then follows an insulating layer of thickness 40 nm, and finally the metallic gates of thickness 60 nm.

A trijunction is a complex Majorana device that can be implemented on a 2DEG by selectively depositing electrostatic gates. It contains two main regions: three nanowires and a semiconducting cavity. We focus on the design of a gate defined triangular cavity. We do not consider the electrostatic modeling of the nanowires since one can assume that the electric field in the nanowires is screened by the superconductor.

The gates are placed in a single layer above the 2DEG with a dielectric layer in between. Different layer configurations were explored, and a single layer is found to be the best in terms of shape-resolution and voltage range. The thickness of each layer determines how

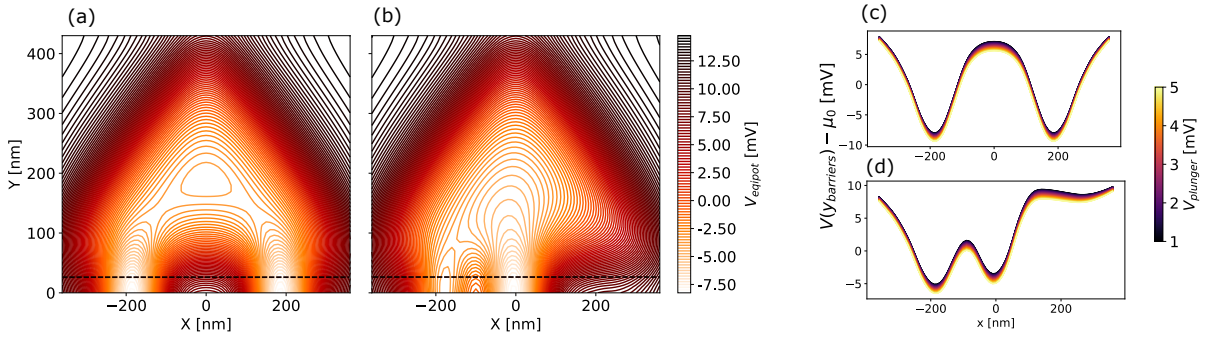

Figure 3.2: Equipotential lines inside the device for representative parameters of the (a) left and right MBS pair and (b) left and center MBS pair. Colorbar indicates value of equipotential lines. (c-d) Cut of the potential along the tunnel barriers, i.e. dashed black lines in (a) and (b), taken for a range of plunger gate voltages. Colorbar in (c-d) indicates the plunger gate voltage.

much the electric field penetrates into the 2DEG. We consider typical parameters from experiments as described in the inset of Fig. 3.1.

In contrast to the geometrical model discussed in the previous chapter, the trijunction is defined in a smooth potential landscape. The global potential is affected by all involved gates. There are three kinds of gates:

1. Plunger gate: Defines and controls the potential inside the triangular cavity region.

2. Screen gates: There are two kinds of screen gates. First, the triangular screen gates deplete the 2DEG around the plunger gate, which contributes to the overall triangular shape. Second, the screen barrier gates between the tunnel gates that keep each nanowire channel separated from the others.

3. Barrier gates: Modulate the coupling between each nanowire and the cavity. They allow to tune the system in the insulating, tunnelling, and strong coupling regimes.

We envision an operation procedure that is a simple as possible, and therefore we consider an operation that varies the minimum number of gates. We tune this device by tuning first the barrier gates such that one of the wires remain disconnected. Then the screen gates in order to deplete the region around the plunger gate. Finally, we tune the plunger gate in order to probe how different cavity state mediate the MBS coupling.

3.2. Device 1

In this section we describe the operation of the gate configuration shown in Fig. 3.1 (a). In Fig. 3.2 (a) - (b) one can observe the potential inside the 2DEG for the coupling of each pair. One can observe that the triangular walls are well defined in the potential, but inside the triangle the bottom of the potential has a different shape.

In Fig. 3.2 (c) and (d) one can observe that a double well is created when coupling a given pair of MBS. For the left and right MBS pair (Fig. 3.2 (c)) the potentials remain well separated. On the other hand, the central pairs are very close (Fig. 3.2 (d)) and the screen barrier can be lowered below the MBS potential, allowing for direct coupling.

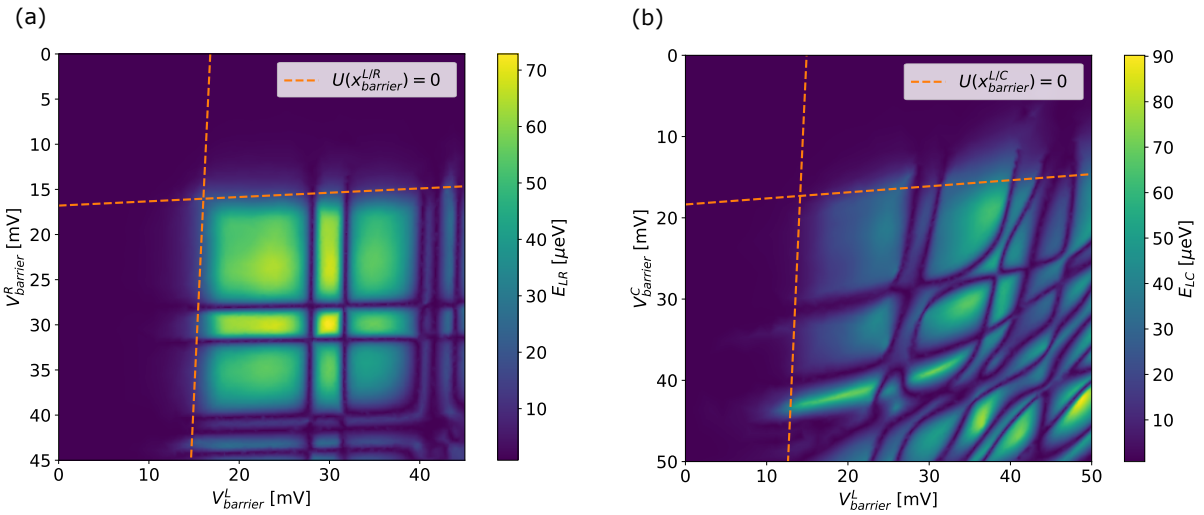

Figure 3.3: Coupling of (a) left and right MBS pair and (b) left and central MBS pair as a function of the corresponding barrier gates in device 1. Orange lines indicate when the potential at the bottom of the barriers crosses 0 V. Plunger gate is tuned around the first resonance. Gate voltages used correspond to those described in Table 3.1.

3.2.1. Barrier gates tuning

Operating the left and right tunnel barriers is straightforward since they are far from each other. Consequently, there is no interdependence between them as can be observed in Fig. 3.3 (a). On the other hand, the operation of the central pairs is not symmetric given the mutual influence of successive barrier gates. In Fig. 3.3 (b) one can observe that the slope of the potential crossings suggests a mutual interaction between successive barrier gates.

The system can be tuned in the insulating, tunnelling, and strong coupling regimes by manipulating the barrier gates. The orange line in Fig. 3.3 indicate the value of the potential at the bottom of the barrier gates with respect to 0. For small voltages, the nanowires are disconnected. As the voltage increases around the orange line, the system enters into the tunnelling regime. In this regime, the coupling is mediated by direct overlap of the MBS wavefunctions. Therefore, one observes a difference in the tunnelling regime of panels (a) and (b) since in the later the MBS are closer. The orange lines indicate the start of the strong coupling regime.

As the barriers are lowered, there are two new effects: On one hand, new crossings caused by resonant cavity levels appear. On the other hand, for very large barrier gates, the MBS couple directly. The former effect can be seen clearly in panel (a) as the two crossings in the strong coupling regime. The later can be seen in the lower right part of panel (b) where the coupling increases due to direct coupling. Keeping the barrier potential as small as possible within strong coupling decreases the influence of these effects.

3.2.2. Screen gates tuning

In Fig. 3.4 one can observe the MBS coupling as a function of the voltages of the two triangular screen gates for each pair. As mentioned before, these gates deplete the regions surrounding the plunger gate and contribute to the triangular shape resolution.

The triangular screen gates allow to tune the device in three different regimes. First, in Fig. 3.4 (a) and (b) one observes that below the orange lines, there some resonances with a small MBS coupling. In this case, electrons can move over the whole 2DEG and

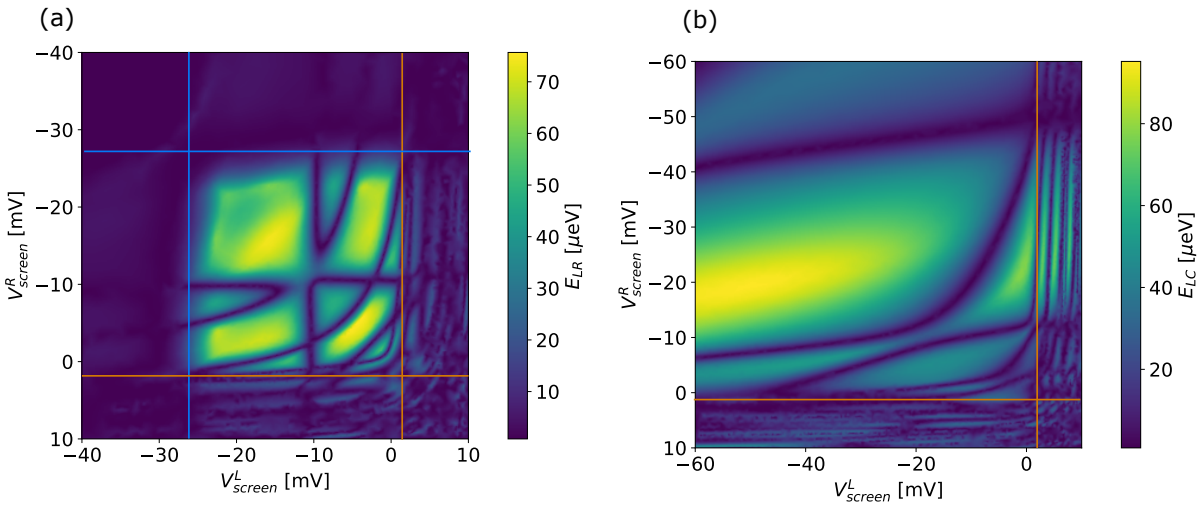

Figure 3.4: Coupling (a) left and right MBS pair and (b) left and central MBS pair as a function of the triangular screen gates in device 1. Three regimes of the depletion are separated by the orange and blue lines. Plunger gate is tuned around the first resonance. Gate voltages used correspond to those described in Table 3.1.

are not confined below the plunger gate. By tuning the potential to more negative values, between the orange and blue lines, a region with large coupling develops, indicating that electrons are confined in the triangular region. Further increasing the potential depletes the area under the plunger gate as can be seen beyond the blue line, i.e. the plunger gate is depleted. Observe that higher voltages are required to reach this last regime in Fig. 3.4 (b).

In Fig. 3.4 (a) one observes that the case of the left and right MBS pair is symmetric. On the other hand, in Fig. 3.4 (b) one observes an asymmetry for the left and central MBS pair. In fact, the coupling increases by tuning one screen gate more negative than the other. This is new regime for the coupling of the central MBS pairs that is not found in the purely geometric model. One can understand this phenomenon as an effectively size decrease for the cavity while maintaining the triangular shape.

3.3. Device 2

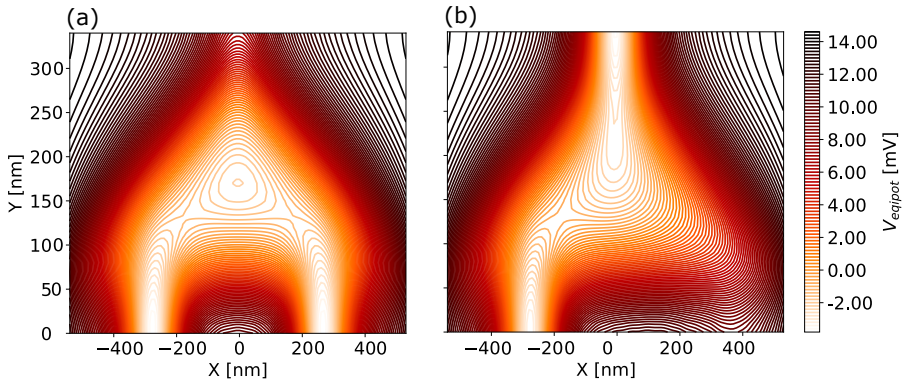

Figure 3.5: Equipotential lines inside the device for representative parameters of the (a) left and right MBS pair and (b) left and center MBS pair. Colorbar indicates value of equipotential lines. (c) Cut of the potential along the tunnel barriers, i.e. dashed black lines in (a) and (b), taken for a range of plunger gate voltages. Colorbar in (c) indicates the plunger gate voltage.

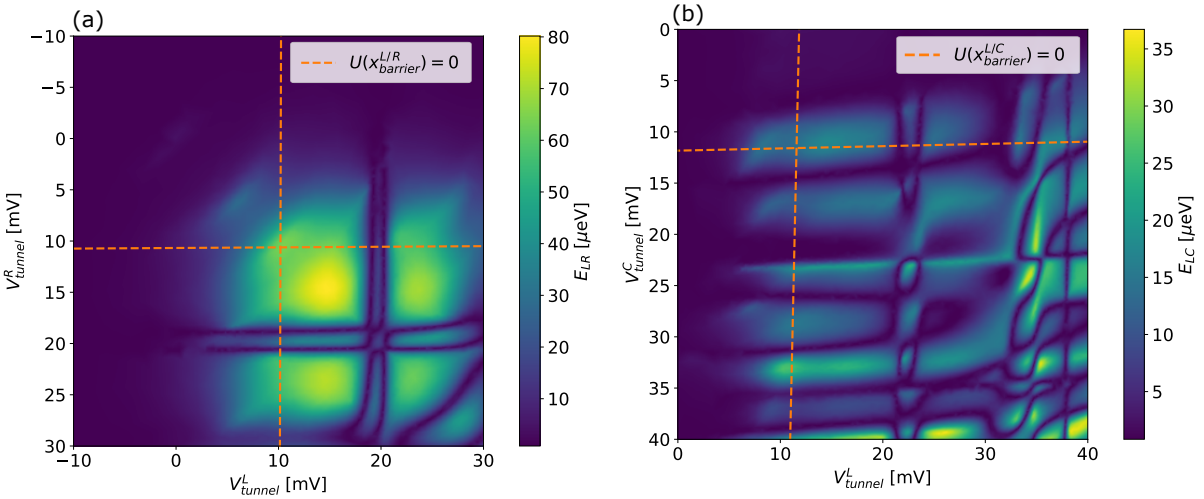

Figure 3.6: Coupling (a) left and right MBS pair and (b) left and central MBS pair as a function of the corresponding barrier gates in device 2. Plunger gate is tuned around the first resonance. Gate voltages used correspond to those described in Table 3.2.

In this section we describe the operation of the gate configuration shown in Fig. 3.1 (b). In contrast to the previous device, here the interplay between barrier and screen gates is crucial to keep the nanowires connected to the cavity. In Fig. 3.5 (a) - (b) one can observe the potential inside the 2DEG for connecting each pair. One observes that the barrier gates are well separated from each other, but the depletion region below the barrier gates depends on the surrounding screen gates as in the case of the top barrier in Fig. 3.5 (b). Furthermore, in panel (b) one can observe that the potential minima inside the cavity follows a narrow channel trajectory. The far disconnected end of the triangular potential is higher, which implies a large deformation from the geometrical case.

3.3.1. Barrier gates tuning

There are two differences with respect to the previous device: First, since all barrier gates remain well separated from each other, there is no interdependence of barrier gates for any pair as one can observe in Fig. 3.6. Second, in the tunnelling regime, there is a significant coupling due to wavefunction overlap. This is a consequence of how the gate geometry influences the spatial distribution of the cavity states.

Since this device has a smaller angle, it resembles a quasi-one dimensional shape. Observe that the dimension of the plunger gate are 800 nm long and 200 nm wide. The wavefunctions will concentrate around the center of the cavity and not in the narrow edges. Consequently, one observes a larger coupling in the tunnelling regime due to resonant trapping for the left and right MBS coupling.

In the strong coupling regime (below orange line in Fig. 3.6) there is a large difference between the coupling of the different pairs. One can observe that Fig. 3.6 (a) is similar to the previous device, which suggests that the triangular geometry effects are present in both devices. On the other hand, Fig. 3.6 (b) shows a smaller coupling in contrast to the purely geometric model. This difference arises from the new structure of the cavity created by the gates. Furthermore, a new set of resonances appears with a non-trivial dependence in both tunnel barriers.

3.3.2. Screen gates tuning

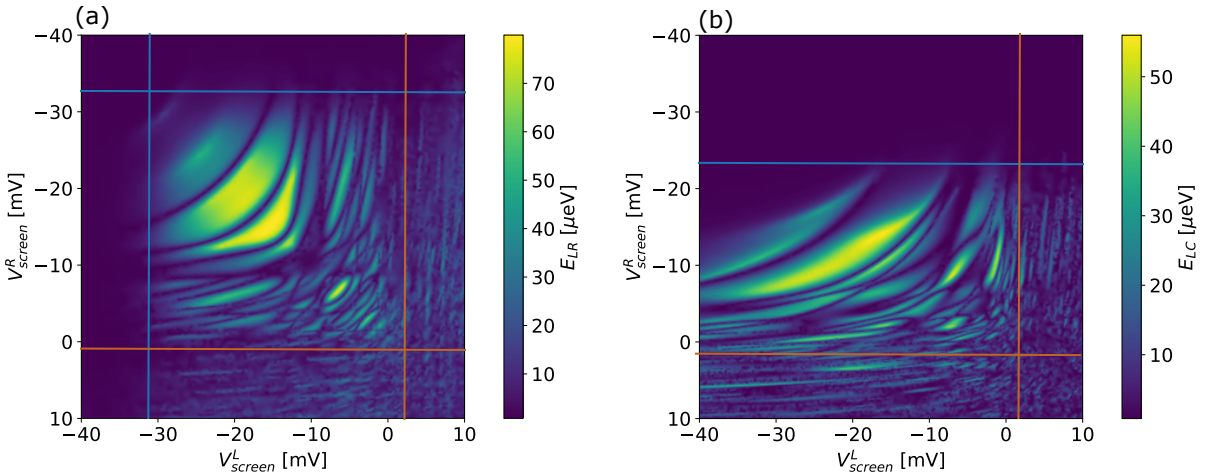

Figure 3.7: Coupling of (a) left and right MBS pair and (b) left and central MBS pair as a function of the triangular screen gates in device 2. Three regimes of the depletion are separated by the orange and blue lines. Plunger gate is tuned around the first resonance. Gate voltages described in Table 3.2.

As in the previous device, the coupling is larger when the region around the plunger gate is depleted than when electron delocalise over the 2DEG. One can observe this in the separate regions shown in Fig. 3.7 marked by the blue and orange lines. In Fig. 3.7 (a) one observes that there is a region where the coupling for the left and right MBS pair has a series of large resonances. By tuning the screen gates inside one of them, the magnitude of the coupling is similar to the previous device.

As mentioned before, the position of the barrier gates is modulated by the screen gates. One can observe in Fig. 3.7 (a) that for voltages above the blue line one of the nanowires disconnects from the cavity. On the other hand, in in Fig. 3.7 (b) one observes the dependence on the screen gates is asymmetric. In this case, the right screen gate disconnects the top nanowire at a voltage smaller than the lower gates. Finally, the region below the orange lines indicates that there is a non-zero coupling for when electrons delocalised over the 2DEG, but no distinguishable pattern is found.

In this device is possible to reach a maximum coupling by properly tuning the screen and barrier gates. The gates design does not allow to explore cases beyond the triangular cavity as in the previous device. In fact, tuning of the screen gates is required for each pair to operate properly.

3.4. Devices operation

In the previous discussion we have described the optimal point for operating each the devices considered. In this section we tune the devices to the operational point described in Tables 3.1 anad 3.2. Then we calculate the MBS coupling as a function of the plunger gate and the result is shown in Fig. 3.8. By observing Fig. 3.8 (a), we can see that the coupling of the different MBS pairs is close to the maximum coupling around $V_{plunger} = 2$meV for the first device. On the other hand, Fig. 3.8 (b) shows that the coupling of different pairs in the second device is highly asymmetric. A maximum can be found for all pairs around $V_{plunger} = 6.5$ meV. However, there is a difference of about 30 meV for the coupling of different pairs in this device.

The shape of the spectra for both MBS pairs in device 1 (Fig. 3.8 (a)) is similar, but the central pair has a larger level spacing. This support the idea that the deformation of the triangular cavity leads to an effective size reduction that involves only the relevant pairs. On the other hand, in Fig. 3.8 (b) one observes a region where the coupling has a peak for the left and right pair, but it has a dip for central pairs.

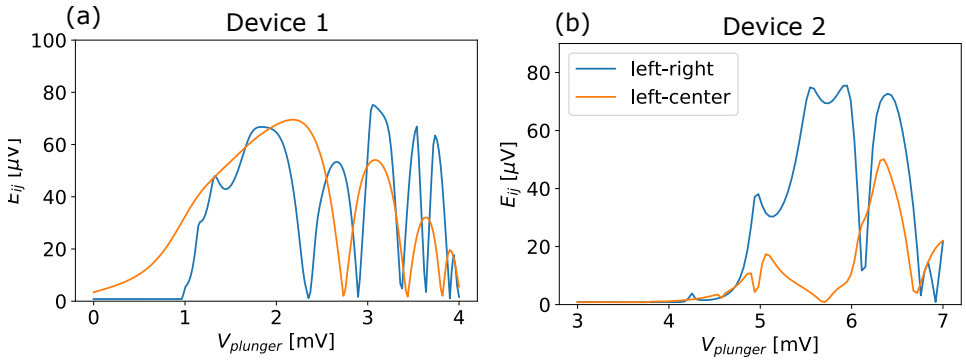

Figure 3.8: MBS coupling of all relevant pairs for each device tuned accordingly to the parameters described in Table 3.1 and Table 3.2.

Both devices are operated by changing three gate voltages at a time to tune between each MBS pair. First of all, the barrier gates are required to connect or disconnect nanowires from the cavity. Tuning between different pairs requires to disconnect one wire while connect a new one. The largest voltage difference in the tuning comes from the barrier gates. Then, the screen gates are tuned such that the region around the plunger gate is depleted. Further tuning for the central pairs is required as was discussed in Fig. 3.4 (b). The set of gate voltages that define the operational point of the devices are shown in Table 3.1 and Table 3.2.

	$V^L_{barrier}$	$V^R_{barrier}$	$V^C_{barrier}$	V^L_{screen}	V^R_{screen}
left-right	35	35	-20	-15	-15
left-center	35	-20	20	-15	40
center-right	-20	35	20	40	-15

Table 3.1: Optimal gate configuration of device 1 shown in Fig. 3.1(a). Voltage units are meV. Remaining gate voltages are fixed: screen barriers between nanowires -30 meV, screen barriers around nanowires -15 meV.

	$V^L_{barrier}$	$V^R_{barrier}$	$V^C_{barrier}$	V^L_{screen}	V^R_{screen}
left-right	17	17	-20	-15	-15
left-center	17	-20	17	-10	-20
center-right	-20	17	17	-20	-10

Table 3.2: Optimal gate configuration of device 2 shown in Fig. 3.1(b). Voltage units are meV. Remaining gate voltages are fixed: screen barriers between nanowires -30 meV, screen barriers around nanowires -15 meV.

4

Conclusions

In this work we have demonstrated that the question of designing an optimal trijunction of Majorana nanowires requires consideration of geometric, and electrostatic details. We have not answered the question of what is the optimal geometry, but we have made progress by analysing different geometries in 1D and 2D.

We have found a systematic difference between different cavity geometries. In quasi-1D cavities, there is a clear behaviour of the different geometries considered. On the other hand, 2D systems show a complex behaviour where device size and shape influence the coupling and shape resolution. Overall, the ring and the triangular geometry have the largest coupling in terms of resonance peak hight and width.

The implementation of a gate-defined trijunction requires a systematic tuning of the device. We have found that the geometric description holds for two-dimensional shapes. However, as the system size decreases, electrostatics dominate over the purely geometrical effects. Nevertheless, a gate-defined shape can be further optimised by deforming the shape of the cavity in a new gate voltage regime.

This work can be extended in three possible ways: On the one hand, further geometry analysis can be used to find the optimal cavity shape that will be later implemented with an electrostatic model. On the other hand, include a measurement protocol that allows to measure the state encoded by the MBS. This is a necessary ingredient in order to design a Majorana qubit. Finally, both previous approaches require the inclusion of disorder effects to have a realistic description

The implementation of a gate-defined ring geometry remains as an open question. The main problem that we found with this geometry is that the coupling between different pairs is highly asymmetric due to resonant trapping. Nevertheless, this problem can be circumvent by defining multiple regions along the ring that can be activated or depleted depending on the pair to couple.

Another possible extension is to implement an optimisation algorithm that determines the optimal shape of the cavity. To consider all pairs simultaneously, one can optimise the minimum coupling. This thesis can be used to establish the constraints on the algorithm, such as device size and nanowire separation. Once the shape is found, an electrostatic implementation is required to determine the feasibility of such result.

Bibliography

[1] J. Alicea, Y. Oreg, G. Refael, F. V. Oppen, and M. P. Fisher. Non-abelian statistics and topological quantum information processing in 1d wire networks. *Nature Physics*, 7:412–417, 2011.

[2] A. E. Antipov, A. Bargerbos, G. W. Winkler, B. Bauer, E. Rossi, and R. M. Lutchyn. Effects of gate-induced electric fields on semiconductor majorana nanowires. *Physical Review X*, 8:31041, 2018.

[3] P. Armagnat, A. Lacerda-Santos, B. Rossignol, C. Groth, and X. Waintal. The self-consistent quantum-electrostatic problem in strongly non-linear regime. *SciPost Physics*, 7, 9 2019.

[4] B. Bauer, T. Karzig, R. V. Mishmash, A. E. Antipov, and J. Alicea. Dynamics of majorana-based qubits operated with an array of tunable gates. *SciPost Physics*, 5:1–20, 2018.

[5] C. W. Groth, M. Wimmer, A. R. Akhmerov, and X. Waintal. Kwant: A software package for quantum transport. *New Journal of Physics*, 16:1–19, 2014.

[6] M. Hell, K. Flensberg, and M. Leijnse. Coupling and braiding majorana bound states in networks defined in proximate two-dimensional electron gases. *Physical Review B*, 96:1–18, 2017.

[7] R. L. O. het Veld, D. Xu, V. Schaller, M. A. Verheijen, S. M. Peters, J. Jung, C. Tong, Q. Wang, M. W. de Moor, B. Hesselmann, K. Vermeulen, J. D. Bommer, J. S. Lee, A. Sarikov, M. Pendharkar, A. Marzegalli, S. Koelling, L. P. Kouwenhoven, L. Miglio, C. J. Palmstrøm, H. Zhang, and E. P. Bakkers. In-plane selective area insb–al nanowire quantum networks. *Communications Physics*, 3, 2020.

[8] A. Y. Kitaev. Unpaired majorana fermions in quantum wires. *Physics-Uspekhi*, 2000.

[9] M. Kjaergaard, F. Nichele, H. J. Suominen, M. P. Nowak, M. Wimmer, A. R. Akhmerov, J. A. Folk, K. Flensberg, J. Shabani, C. J. Palmstrom, and C. M. Marcus. Quantized conductance doubling and hard gap in a two-dimensional semiconductor-superconductor heterostructure. *Nature Communications*, 3 2016.

[10] T. Laeven, B. Nijholt, M. Wimmer, and A. R. Akhmerov. Enhanced proximity effect in zigzag-shaped majorana josephson junctions. *Physical Review Letters*, 3 2019.

[11] M. Leijnse and K. Flensberg. Introduction to topological superconductivity and majorana fermions. *Semiconductor Science and Technology*, 27, 2012.

[12] C. X. Liu, J. D. Sau, and S. D. Sarma. Distinguishing topological majorana bound states from trivial andreev bound states: Proposed tests through differential tunneling conductance spectroscopy. *Physical Review B*, 97:1–8, 2018.

[13] R. M. Lutchyn, T. Stanescu, and S. D. Sarma. Search for majorana fermions in multiband semiconducting nanowires. *Physical Review Letters*, 8 2010.

[14] C. M. Moehle, C. T. Ke, Q. Wang, C. Thomas, D. Xiao, S. Karwal, M. Lodari, V. van de Kerkhof, R. Termaat, G. C. Gardner, G. Scappucci, M. J. Manfra, and S. Goswami. Insbas two-dimensional electron gases as a platform for topological superconductivity. 5 2021.

[15] R. G. Nazmitdinov, R. G. Nazmitdinov, K. N. Pichugin, K. N. Pichugin, I. Rotter, P. Šeba, and P. Šeba. Conductance of open quantum billiards and classical trajectories. *Physical Review B - Condensed Matter and Materials Physics*, 66:853221–8532213, 2002.

[16] R. G. Nazmitdinov, K. N. Pichugin, I. Rotter, and P. Šeba. Whispering gallery modes in open quantum billiards. *Physical Review E - Statistical Physics, Plasmas, Fluids, and Related Interdisciplinary Topics*, 64:5, 2001.

[17] C. Reeg, D. Loss, and J. Klinovaja. Metallization of a rashba wire by a superconducting layer in the strong-proximity regime. *Physical Review B*, 97, 2018.

[18] J. D. Sau, D. J. Clarke, and S. Tewari. Controlling non-abelian statistics of majorana fermions in semiconductor nanowires. *Physical Review B - Condensed Matter and Materials Physics*, 84:1–8, 2011.

[19] J. Shabani, M. Kjaergaard, H. J. Suominen, Y. Kim, F. Nichele, K. Pakrouski, T. Stankevic, R. M. Lutchyn, P. Krogstrup, R. Feidenhans'l, S. Kraemer, C. Nayak, M. Troyer, C. M. Marcus, and C. J. Palmstrøm. Two-dimensional epitaxial superconductor-semiconductor heterostructures: A platform for topological superconducting networks. *Physical Review B*, 11 2015.

[20] H. J. Suominen, M. Kjaergaard, A. R. Hamilton, J. Shabani, C. J. Palmstrøm, C. M. Marcus, and F. Nichele. Zero-energy modes from coalescing andreev states in a two-dimensional semiconductor-superconductor hybrid platform. *Physical Review Letters*, 3 2017.

[21] B. M. Terhal and D. P. Divincenzo. Classical simulation of noninteracting-fermion quantum circuits, 2001.

[22] A. Vuik, B. Nijholt, A. Akhmerov, and M. Wimmer. Reproducing topological properties with quasi-majorana states. *SciPost Physics*, 7:1–13, 2019.

[23] L. Wirtz, J. Z. Tang, and J. Burgdörfer. Geometry-dependent scattering through ballistic microstructures: Semiclassical theory beyond the stationary-phase approximation. *Physical Review B - Condensed Matter and Materials Physics*, 56:7589–7597, 1997.